ARTICLES

Photoluminescence Properties of SnO_2 Nanoparticles Synthesized by Sol−Gel Method

Feng Gu, Shu Fen Wang, Meng Kai Lü,* Guang Jun Zhou, Dong Xu, and Duo Rong Yuan

State Key Laboratory of Crystal Materials, Shandong University, Jinan 250100, P. R. China

Received: September 15, 2003; In Final Form: March 3, 2004

Nanocrystalline SnO_2 particles have been synthesized by a simple sol−gel method. The structural and optical properties of these SnO_2 particles are investigated using X-ray powder diffraction, transmission electron microscopy, UV−visible absorption, and photoluminescence spectroscopy. The oxygen-vacancies-related photoluminescence of pure, cerium-, and manganese-doped SnO_2 nanoparticles was systematically investigated. The origin of the luminescence is assigned to the recombination of electrons in a conduction band with holes in the $V_o^{\bullet\bullet}$ center. Experimental results reveal that increasing calcining temperature can decrease the oxygen-vacancies-related luminescence intensity of the sample. After introducing Ce^{3+}/Mn^{2+} ions into the host, the oxygen-vacancies-related luminescence has been enhanced remarkably resulting from the formation of many more oxygen vacancies. The dependence of the oxygen-vacancies-related luminescence intensity on the Ce^{3+}/Mn^{2+} concentration is also discussed.

Introduction

The optical properties of nanocrystalline semiconductors have been studied extensively in recent years. If the particle size of a semiconductor becomes comparable to the Bohr radius of the exciton, the ratio of surface atoms to those in the interior increases remarkably, leading to the surface properties playing an important role in the properties of the material. Semiconductor nanoparticles also exhibit a change in their electronic properties relative to that of the bulk counterpart, as the size of the solid becomes smaller, the band gap becomes larger. These quantum size effects have stimulated great interest in both basic and applied research.[1−4]

Owing to their unique electronic, magnetic, and optical properties, semiconductor nanoparticles may find wide applications in various fields, such as microelectronics, photocatalysis, nonlinear optics, photoelectrochemistry, imaging science, and electro-optics. Among the various semiconductor materials, SnO_2 is a prototypical optically transparent n-type semiconductor with a wide band gap ($E_g = 3.62$ eV at 300 K), which spans a wide range of applications such as resistors, gas sensors, special coating for energy-conserving "low-emissivity" windows, transparent heating elements, electrodes in glass melting furnaces, and antistatic coating.[5−8] A variety of methods, such as chemical vapor deposition (CVD), magnetron sputtering, and thermal evaporation, are available to prepare SnO_2 thin films or nanoparticles.[9−11] The synthesis of SnO_2 with one-dimensional (1D) nanostructures with different shapes has also been reported.[12,13]

Recently, considerable research has been focused on the exploration of novel properties of semiconductor nanoparticles, especially the photoluminescent properties.[14] Photoluminescence may reveal the presence of crystalline defects resulting from the synthesis process. With respect to the luminescence of SnO_2 nanoparticles, oxygen vacancies have been assumed to be the most likely candidates for the recombination centers in luminescence processes, which resemble that of other oxide nanocrystals such as ZnO, TiO_2, SiO_2, and Ga_2O_3.[15−18] Though, it is known that oxygen vacancies play an important role in luminescence processes in SnO_2 nanoparticles, it is interesting to study the effect of defects formed by the addition of impurity ions on the luminescence processes. In the present paper, we select Ce^{3+} and Mn^{2+} ions as the impurity dopants in the study of oxygen-vacancies-related luminescence of nanocrystalline SnO_2 particles. To our knowledge, few researches have been emphasized on this point. The Ce^{3+} ion has a very simple electron configuration, whose 4f−5d transitions are allowed and sensitive to changes in the crystal field.[19,20] Mn^{2+}-doped ZnS nanoparticles have been successfully investigated, and Mn^{2+} emission has been observed following band gap excitation.[21,22] Usually when a trivalent/divalent Ce^{3+}/Mn^{2+} ion sits in a Sn^{4+} site, an increase in the number of oxygen vacancies would be expected, producing oxygen-vacancies-related traps that make a contribution to the luminescence. Further, it offers an opportunity to factually reveal the relationship between the phase structure and luminescence processes.

Experimental Section

Sample Preparation. Tin oxide nanoparticles were prepared by a simple sol−gel method. The initial composition was $Sn_{1-x}M_xO_2$ ($M = Ce^{3+}$, Mn^{2+}, $x = 0-0.05$). After 10.00 g of tin chloride (hydrous $SnCl_4 \cdot 5H_2O$ (A.R.)) and the proper amount of cerium/manganese chloride solution ($CeCl_3$, 0.1 M; $MnCl_2$, 0.1 M) were dissolved in distilled water, an aqueous ammonia solution (2 M) was added to the above solution dropwise. The dropping rate must be well controlled for the chemical homogeneity. The critical pH of this reaction was kept at 4. The condensation reaction led to the formation of polymeric local

* To whom correspondence should be addressed. E-mail: mengkailu@icm.sdu.edu.cn.

10.1021/jp036741e CCC: $27.50
Published on Web 05/25/2004

structure within the sol particles with a Sn (Ce/Mn)−O−Sn band. Subsequently, the resultant sol was filtered using distilled water to eliminate the chlorine ions in the system, and was heated at 80 °C for several hours until completely gelled to obtain homogeneous smaller gel particles. These dry gel particles were calcined in an air atmosphere at 400−600 °C for 2 h to remove the inorganic groups.

Characterization. The X-ray diffraction (XRD) patterns of the samples were measured by using a Japan RigaKu D/MAX 2200PC diffractometer with Cu−Kα radiation (λ = 0.15418 nm) and a graphite monochromator. The crystallite size D of the prepared powders was estimated using the Scherrer equation as follows[23]

$$D = \frac{0.9\lambda}{\beta \cos \theta} \tag{1}$$

where λ, β, and θ are the X-ray wavelength (0.15418 nm for Cu−Kα), Bragg diffraction angle, and the full width at half-maximum of the diffraction peak (fwhm), respectively. Furthermore, it is known that fwhm can be interpreted in terms of lattice strain and crystalline size,[24,25] which can be expressed by the following equation

$$\frac{\beta \cos \theta}{\lambda} = \frac{1}{\epsilon} + \frac{\eta \sin \theta}{\lambda} \tag{2}$$

where ϵ and η are the effective particle size and the effective strain. The effective particle size taking strain into account can be estimated by plotting $\beta \cos \theta/\lambda$ versus $\sin \theta/\lambda$.

Transmission electron micrograph (TEM) images were taken with a JEM-100CX transmission electron microscope. Samples for the TEM were prepared by ultrasonically dispersing the product in ethanol, and then droplets were placed on carbon-coated Cu grids. The excitation and photoluminescence (PL) spectra of the sample were measured with a Hitachi M-850 fluorescence spectrometer.

UV−vis absorption spectra were recorded using a spectrophotometer (U-3500) with a 1-cm quartz cell at room temperature. The colloid solutions in isopropyl alcohol were prepared ultrasonically for the UV−vis measurements. The band gap energy E_g for the SnO_2 nanoparticles can be determined by extrapolation to the zero absorption coefficient which is calculated from the following equation

$$\alpha = \frac{2303A\rho}{lC} \tag{3}$$

where A is the absorbance of a sample; ρ is the density of SnO_2; C is the concentration of the particles; and l is the optical path length. The optical absorption coefficient α of a semiconductor close to the band edge can be expressed by the following equation[26]

$$\alpha = \frac{K(h\nu - E_g)^n}{h\nu} \tag{4}$$

where K is a constant, E_g is the band gap, and n is a value that depends on the nature of the transition. In this case, n is equal to $^1/_2$ for this direct allowed transition. The band gap can be estimated from a plot of $(\alpha h\nu)^2$ versus photon energy.

Results and Discussion

Figure 1 gives the XRD patterns of the SnO_2 particles obtained at different calcining temperatures from 400 to 600 °C for 2 h. All the diffraction lines are assigned well to tetragonal rutile crystalline phases of tin oxide with a reference pattern (JCPDS 41-1445). The presence of broad peaks indicates the SnO_2 has a very small crystalline size, or SnO_2 particles are semicrystalline in nature.[27] It is also found that the XRD peaks become gradually sharper with increasing temperature, indicating the particle grew larger in size. The crystallite sizes determined from the Scherrer equation are 2.8, 4.2, and 8.8 nm, respectively. Due to a very small crystalline size in nanoscale, lattice strain can be expected from the prepared SnO_2 nanoparticles. In Figure 2, $\beta \cos \theta/\lambda$ is plotted versus $\sin \theta/\lambda$ for the particle sizes of samples calcined at 400, 500 and 600 °C, respectively. The effective particle size taking the strain into account can be estimated from the extrapolation of the plots, which is similar to that calculated from Scherrer's equation (shown in Table 1). The negative slope of the fitted lines indicates the presence of compressive strain in the SnO_2 crystal lattice. As the calcining temperature increases, the decrease of the fwhm of the diffraction peaks results in the decrease of the slope, indicating the strain in the SnO_2 host lattice diminishes gradually.[25] Therefore, prominent surface and strain forces resulting from the compression of the SnO_2 lattice can be expected, which would have important effects on the optical properties of the SnO_2 nanoparticles.

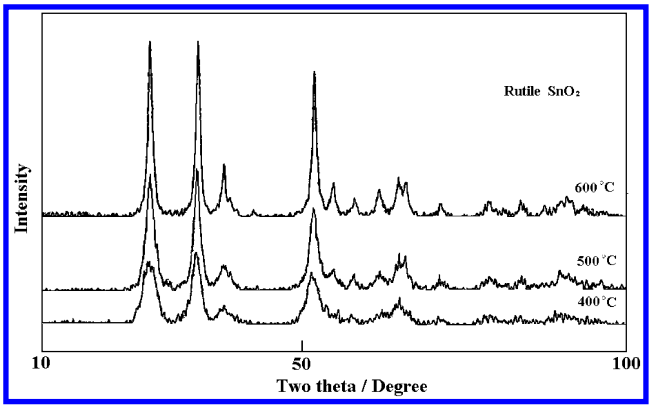

Figure 1. XRD patterns for SnO_2 particles calcined at different temperatures.

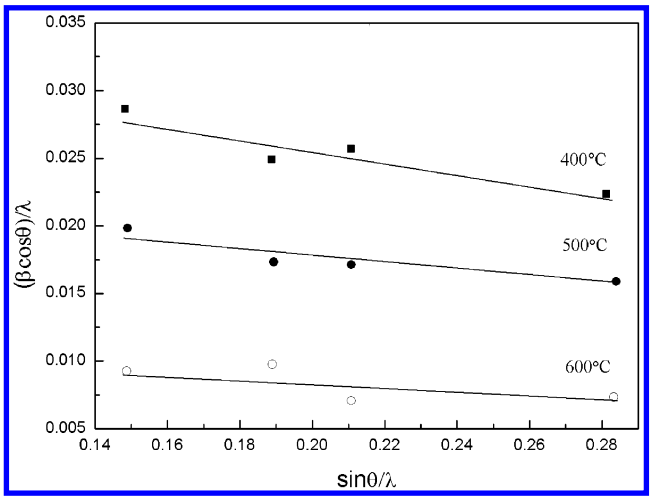

Figure 2. $\beta \cos \theta/\lambda$ vs $\sin \theta/\lambda$ for the prepared SnO_2 nanoparticles calcined at 400, 500, and 600 °C, respectively.

The TEM observation for the as-prepared SnO_2 particles calcined at 400 °C is shown in Figure 3. It is apparent that the SnO_2 nanoparicles are ultra-fine and the particle size of these nanoparticles is about 3 nm, which is coincident with the size of particles calculated from the Scherrer equation.

TABLE 1: Summary of the Physical Characterization of Sol−Gel Derived SnO_2 Nanoparticles

						PL intensity at 400 nm/(a.u.)[e]		
sample	temp/°C	D_1[a]/nm	D_2[b]/nm	η[c] (10^{-2})	E_g[d]/eV	undoped	Mn-doped	Ce-doped
1	400	2.8	2.9	4.32	4.2	340	728	1596
2	500	4.2	4.3	2.39	3.9	220	399	828
3	600	8.8	9.0	1.24	3.7	180	262	421

[a] D_1 is estimated from the Scherrer equation. [b] D_2 is the effective particle size taking the strain into account. [c] η is the lattice strain. [d] E_g is the band gap energy from UV absorption spectra. [e] The excitation wavelength was 300 nm (C_{Mn} = 3%, C_{Ce} = 2%).

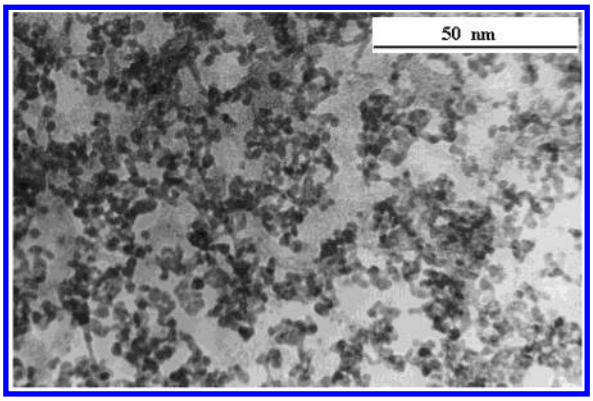

Figure 3. TEM micrograph of the as-prepared SnO_2 nanoparticles calcined at 400 °C for 2 h.

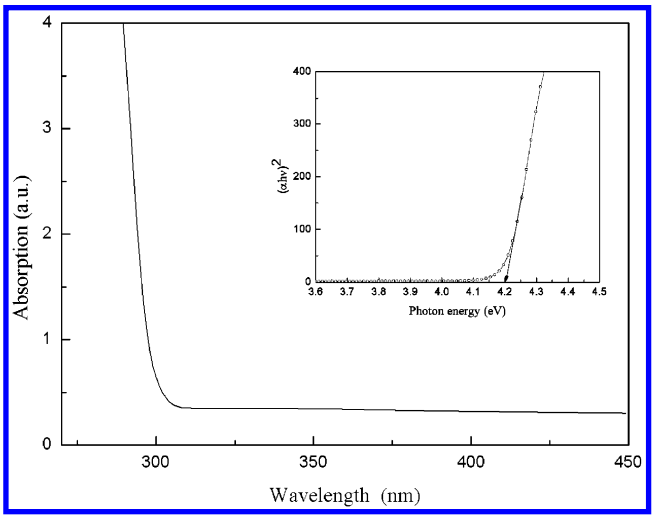

Figure 4. Absorption spectrum for the SnO_2 nanoparticles calcined at 400 °C. The inset shows the corresponding plot of $(\alpha h\nu)^2$ vs photon energy for the SnO_2 nanoparticles.

For semiconductor nanoparticles, the quantum confinement effect is expected. Semiconductor nanoparticles with dimensions in the order of the bulk excition will show unique optical properties, which depend strongly on the size. In semiconductors, band gaps have been found to be particle size dependent. The band gap increases with decreasing particle size, and the absorption edge will be shifted to a higher energy concomitantly. The absorption spectrum of SnO_2 nanoparticles calcined at 400 °C is shown in Figure 4, and the value of the absorption onset of the sample is 300 nm. The absorption onset appears red shifted upon particle growth, indicating that the particles are really in the quantum regime. The band gap energy E_g for the SnO_2 nanoparticles can be determined by extrapolation to the zero absorption coefficient which is calculated from eq 4. The intercept of the tangent to the plot will give a good approximation of the band gap energy for this direct band gap material (shown in the inset of Figure 4 for the sample calcined at 400 °C).[28] The band gap of the as-prepared SnO_2 nanoparticles (4.20 eV) is larger than the value of 3.62 eV for the bulk SnO_2. Due

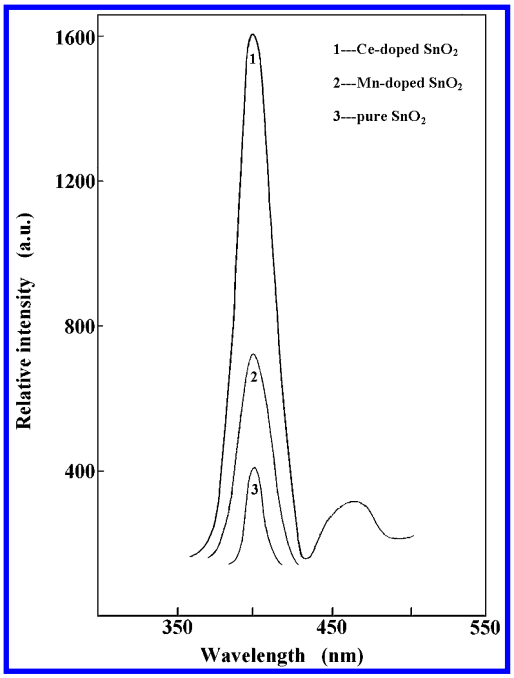

Figure 5. Emission spectra of Ce^{3+}-, Mn^{2+}-doped, and pure SnO_2 nanoparticles calcined at 400 °C for 2 h under excitation at 300 nm (C_{Mn} = 3% and C_{Ce} = 2%).

to the improved grain size for samples calcined at 500 and 600 °C, the band gap gradually shifts toward the value for the macrocrystalline SnO_2, hence the shift in absorption onset (shown in Table 1).

PL emission spectra were recorded for the Ce^{3+}-, Mn^{2+}-doped, and pure SnO_2 samples (shown in Figure 5). The excitation wavelength was 300 nm. In all samples a dominant PL peak was observed at 400 nm. Earlier reports have indicated that SnO_2 thin films exhibited a broad dominant peak near 396 nm.[29] While in the emission spectra of Ce^{3+} -doped samples (C_{Ce} = 2%) a rather weak band centered at 460 nm presents along with the 400 nm emission. The emission of Ce^{3+} usually consists of two bands of the transitions of the 5d-excited state to $^2F_{7/2}$ and $^2F_{5/2}$ states.[19,20,30] The 460 nm emission observed in SnO_2:Ce^{3+} seems to belong to these 5d−4f transitions. With respect to the prominent emission centered at 400 nm, which can be attributed to electron transition mediated by defects levels in the band gap, such as oxygen vacancies, has been enhanced five times larger than that of pure SnO_2 due to the addition of the Ce^{3+} dopant. However, in Mn^{2+}-doped SnO_2 samples (C_{Mn} = 3%), the characteristic peaks of Mn^{2+} ions could not be collected, which differs from that of Ce^{3+} in the SnO_2 host. But the emission intensity at 400 nm is still two times higher than that of the pure sample.

Generally, defects such as oxygen vacancies are known to be the most common defects in oxides and usually act as radiative centers in luminescence processes. Among the oxygen vacancies in the oxide, only the $V_o^{\bullet}$ state observed by EPR is paramagnetic, and it is expected that most oxygen vacancies

will be in their paramagnetic $V_o^{\bullet}$ state under flat-band conditions.[31] In some publications, $V_o^{\bullet}$ is assumed to be the recombination center for the luminescence emission,[32] which has an effective monovalent positive charge with respect to the regular O^{2-} site. Actually, after such a recombination the effectively neutral $V_o^{\times}$ center will be formed, whose energy is very close to the conduction band edge due to the correlation energy of the two electrons.[33] At room temperature, all $V_o^{\times}$ centers are thermally dissociated into $V_o^{\bullet}$ centers and conduction band electrons. Therefore, photons with an energy of 3.1 eV (400 nm) will not be emitted through a transition of an electron from the conduction band to a $V_o^{\bullet}$ level, as such a transition effectively occurs between the conduction band edge and the $V_o^{\times}$ level. However, recombination of a conduction band electron with a $V_o^{\bullet\bullet}$ center (an oxygen vacancy containing no electrons, having an effective divalent positive charge with respect to the normal O^{2-} site) can yield such a blue emission band. Such $V_o^{\bullet\bullet}$ centers can be formed when a hole is trapped at a $V_o^{\bullet}$ center. Thus, a model for this blue emission of the photoexcited SnO_2 nanoparticles can be proposed. The excitation of the SnO_2 nanoparticle starts with the creation of an electron−hole pair. The electron is promoted from the valence band to the conduction band, leaving a hole in the valence band. The active hole formed can be trapped at the $V_o^{\bullet}$ center directly to form the $V_o^{\bullet\bullet}$ center or at the surface of the particle. Then the surface-trapped hole may transfer back into the particle to recombine with an electron in a deep trap ($V_o^{\bullet}$) to form the $V_o^{\bullet\bullet}$ center. Thereafter, recombination of a $V_o^{\bullet\bullet}$ center with a conduction band electron gives rise to the blue emission. Schematically, it can be presented as follows

$$SnO_2 + h\nu \rightarrow SnO_2(e'_{CB} + h^{\bullet}_{VB}) \quad (5)$$

$$V_o^{\bullet} + h^{\bullet}_{VB} \rightarrow V_o^{\bullet\bullet} \quad (6)$$

$$SnO_2(e'_{CB} + h^{\bullet}_{VB}) \rightarrow SnO_2(e'_{CB} + h^{\bullet}_{surface}) \quad (7)$$

$$V_o^{\bullet} + h^{\bullet}_{surface} \rightarrow V_o^{\bullet\bullet} \quad (8)$$

$$V_o^{\bullet\bullet} + e'_{CB} \rightarrow V_o^{\bullet} + h\nu_o \quad (9)$$

Here, surface denotes the surface states of the particles. After photoexcitation, all of the above processes can take place in the SnO_2 nanoparticles. Process 9 is the radiative process, which gives the blue emission. From the above scheme, it is clearly seen that the blue emission band has been generated due to the recombination of the deep trapped charges and photogenerated electrons from the conduction band.

After the addition of Ce^{3+} or Mn^{2+} to the host lattice, the negative charge of the Ce'_{Sn}/Mn''_{Sn} ion has to be compensated for somewhere in the lattice in the form of an oxygen vacancy. By incorporating Ce^{3+} ions into the SnO_2 host lattice, many more $V_o^{\bullet}$ centers are formed to maintain the balance of the valence compared with the initial condition. Subsequently, in the luminescence processes, more holes can be trapped at these $V_o^{\bullet}$ centers to form the recombination center ($V_o^{\bullet\bullet}$ centers) after photoexcitation of the SnO_2 nanoparticles. That is the reason the PL intensity becomes remarkably larger after introducing Ce^{3+} to the SnO_2 host. However, after introducing Mn^{2+} ions to the SnO_2 host the metastable $V_o^{\bullet\bullet}$ centers are created in situ, which will share electrons from tin vacancies nearby to present in the form of a tin−oxygen vacancy pair, and the relative luminescence intensity will increase compared with that of the pure sample due to the simultaneous formation of $V_o^{\bullet}$ centers. However, after introducing Mn^{2+} ions into the host, the nonradiative recombination can occur easily due to the enhanced probability of the interaction of Mn^{2+} ions nearby, originating from the continuous solubility of Mn^{2+} ions in the SnO_2 host.

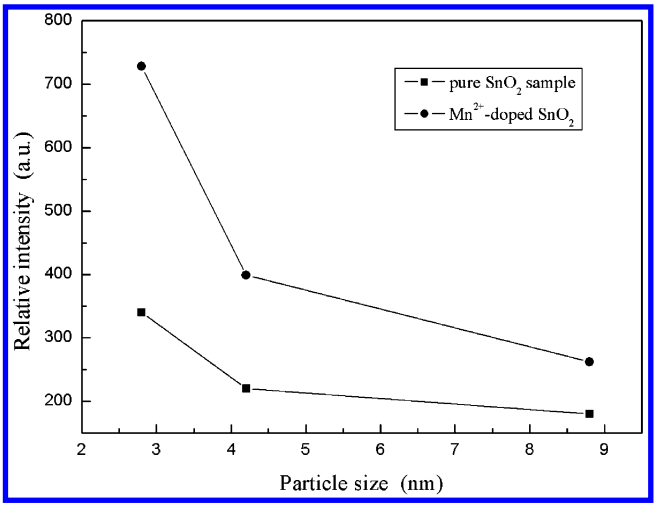

Figure 6. Influence of particle size on relative luminescence intensity of pure and Mn^{2+}-doped and pure SnO_2 samples (C_{Mn} = 3%).

Besides the size quantization, surface effects can strongly influence the optical properties of these SnO_2 nanoparticles. Because of the large surface-to-volume ratio of the present SnO_2 nanoparticles, much unsaturated bonding of the surface atoms is expected at the surface of the particles. So, the surface will play an important role in the quenching of the luminescence. Upon photoexcitation of the SnO_2 nanoparticles, probable candidates for the trapping of holes are O^{2-} ions at the surface. Furthermore, trapping of a photogenerated hole at the surface is also in agreement with the size-dependence of the emission intensities. In Figure 6, we also demonstrate the relative photoluminescence intensity as a function of particle size of the Mn^{2+}-doped and pure SnO_2 samples (also shown in Table 1). As the calcining temperature increases, the particle size of the SnO_2 nanocrystal becomes larger, while the oxygen-vacancies-related luminescence intensity decreases remarkably. This can be attributed to the significant decrease of both the surface defects and concentration of oxygen vacancies of the SnO_2 nanoparticles.[31] Therefore, the rate for a surface trapping process decreases as the particle size increases since the surface-to-volume ratio decreases.

The blue emission is also studied as a function of Ce^{3+} and Mn^{2+} concentration in the SnO_2 nanoparticles (shown in Figure 7). It is found that with increasing Ce^{3+} concentration from 0 to 2%, the PL intensity rose rapidly and reached a maximum. At higher Ce^{3+} concentrations, the intensity started to decrease slowly. Although the exact mechanism for this quenching to occur is still not yet clear, it can be considered that the quenching of the luminescence is associated with the recombination of many more electrons and holes trapped at the surface of the SnO_2 nanoparticles. By introducing Ce^{3+} ions into the SnO_2 host lattice, it is suggested that only a minor fraction of the total amount of Ce^{3+} introduced into the SnO_2 substitutes for the tin positions, which is likely related to the limited "solubility" of the substitutional Ce^{3+} in the SnO_2 matrix. Most of the Ce^{3+} ions may well be precipitated into SnO_2:Ce^{3+} clusters, or even into a separate cerium oxide phase. The excess Ce^{3+} phases will likely reside at surface or grain boundaries to yield optimum strain relief. A similar condition occurs in Sb^{3+}-doped colloidal

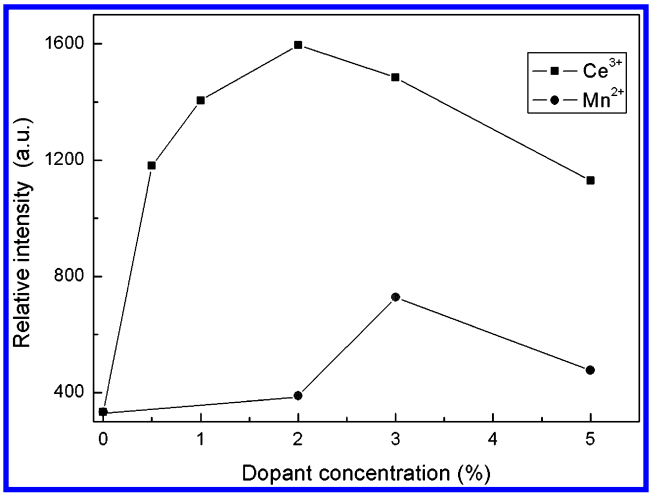

Figure 7. Ce^{3+} and Mn^{2+} concentration dependence of relative luminescence intensity at 400 nm of the SnO_2 samples calcined at 400 °C.

SnO_2 nanoparticles.[34,35] The nonradiative recombination will occur easily after trapping of the hole and electron at the surface of the particles, which can be presented schematically as follows

$$SnO_2(e'_{CB} + h^{\bullet}_{VB}) \rightarrow SnO_2(e'_{surface} + h^{\bullet}_{surface}) \quad (10)$$

$$e'_{surface} + h^{\bullet}_{surface} \rightarrow \text{heat} \quad (11)$$

However, as to Mn^{2+}-doped SnO_2 samples, it is easy for the Mn^{2+} ion to substitute for the Sn^{4+} ion, which can be due to the fact that the radius of Sn^{4+} (0.76 Å) is similar to that of an Mn^{2+} (0.80 Å) ion. It is generally considered that the quenching of the luminescence is associated with interaction among Mn^{2+} ions, and small clusters located on the surface or on the grain boundaries of the nanoparticles,[36] resulting in the recombination of electrons and holes at the surface of the particles for the nonradiative processes.

Conclusions

On the basis of a simple sol−gel process and a careful investigation of the structure, this study systematically discussed the origin of the blue emission and the effect of calcining temperature, impurity ions, and impurity concentration on the oxygen-vacancies-related luminescence of nanocrystalline SnO_2 particles. X-ray diffraction, transmission electron micrographs, and photoluminescence are well correlated with the structural characteristics of the SnO_2 nanoparticles. After introducing Ce^{3+} ions into the host, many more $V_o^{\bullet}$ centers were formed, which capture holes from the valence band to form more recombination centers for the blue emission. Due to the nanometer particle size, rich information can be expected at the surface of the SnO_2 particles, which influences this oxygen-vacancies-related luminescence process greatly.

References and Notes

(1) Henglein, A. *Chem. Rev.* **1989**, *89*, 1861.
(2) Weller, H. *Adv. Mater*. **1993**, *32*, 41.
(3) Hagfeldt, A.; Gratze, M. *Chem. Rev.* **1995**, *95*, 49.
(4) Alivisatos, A. P. *J. Phys. Chem.* **1996**, *100*, 13226.
(5) Ogawa, H.; Abe, A.; Nishikawa, M.; Hayakawa, S. *J. Electrochem. Soc*. **1981**, *128*, 2020.
(6) Arfsten, N. J.; Kaufmann, R.; Dislich, H. *Proceedings of the International Conference on Ultrastructure Processing of Ceramics Glass and Composites*, Gainesville, FL, 1983; Wiley: New York, 1984; p 189.
(7) Jarzebski, Z. M.; Marton, J. P. *J. Electrochem. Soc*. **1976**, *123*, 299c.
(8) Jarzebski, Z. M.; Marton, J. P. *Electrochem. Soc*. **1976**, *123*, 333c.
(9) Tarey, R. D.; Raju, T. A. *Thin Solid Films* **1995**, *128*, 181.
(10) Minami, T.; Nanto, H.; Takata, S. *Jpn. J. Appl. Phys*. **1988**, *27*, L287.
(11) Schlosser, V.; Wind, G. *Proceedings of the 8th EC Photovoltaic Solar Energy Conference*, Florence, Italy, Kluwer Dordrecht, 1998; p 998.
(12) Jian, J. K.; Chen, X. L.; Wang, W. J.; Dai, L.; Xu, Y. P. *Appl. Phys. A* **2003**, *76*, 291.
(13) Liu, Y. K.; Zheng, C. L.; Wang, W. Z.; Yin, C. R.; Wang, G. H. *Adv. Mater*. **2001**, *13*, 1883.
(14) Wang, Y.; Herron, N. *J. Phys. Chem.* **1988**, *92*, 4988.
(15) Gu, F.; Wang, S. F.; Song, C. F.; Lu, M. K.; Qi, Y. X.; Zhou, G. J.; Xu, D.; Yuan, D. R. *Chem. Phys. Lett*. **2003**, *372*, 451.
(16) Vanheusden, K.; Warren, W. L.; Seaeger, C. H.; Jallant, D. R.; Voigt, J. A.; Gnade, B. E. *J. Appl. Phys*. **1996**, *79*, 7983.
(17) Liu, Y. J.; Claus, R. O. *J. Am. Chem. Soc*. **1997**, *119*, 5273.
(18) Zhang, J.; Jiang, F. H. *Chem. Phys*. **2003**, *289*, 243.
(19) Dorenbos, P. *Phys. Rev. B* **2000**, *62*, 15640.
(20) Bettinelli, M.; Moncorge, R. *J. Lumin*. **2001**, *92*, 287.
(21) Bhargava, R. N.; Gallagher, D.; Welker, T. *J. Lumin*. **1994**, *60*, 275.
(22) Bhargav, R. N.; Gallagher, D.; Ilong, X.; Nurmikko, A. *Phys. Rev. Lett*. **1994**, *72*, 416.
(23) Cullity, B. D. *Elements of X-ray Diffractions*; Addition-Wesley: Reading, MA, 1978; p 102.
(24) Oadri, S. B.; Yang, J. P.; Skelton, E. F.; Ratna, B. R. *Appl. Phys. Lett*. **1997**, *70*, 1020.
(25) Williamson, G. K.; Hall, W. H. *Acta Metall*. **1953**, *1*, 22.
(26) Dare-Edwards, M.; Goodenough, J. B.; Hamnett, A.; Trevellick, P. *J. Chem. Soc., Faraday Trans. 1* **1979**, *79*, 2027.
(27) *X-ray Diffraction Procedure*; Klug, H., Alexander, L, Eds.; Wiley: New York, 1962; p125.
(28) Tsunekawa, S.; Fukuda, T.; Kasuya, A. *J. Appl. Phys*. **2000**, *87*, 1319.
(29) Kim, T. W.; Lee, D. U.; Yoon, Y. S. *J. Appl. Phys*. **2000**, *88*, 3759.
(30) Jia, D. D.; Zhu, J.; Wu, B. Q.; E, S. *J. Lumin*. **2001**, *93*, 107.
(31) Vanheusden, K.; Warren, W. L.; Seager, C. H.; Tallant, D. R.; Voigt, J. A.; Gnade, B. E. *J. Appl. Phys*. **1996**, *79*, 7983.
(32) Du, Y.; Zhang, M. S.; Hong, J.; Shen, Y.; Chen, Q.; Yin, Z. *Appl. Phys. A* **2003**, *76*, 171.
(33) Dijken, A.; Meulenkamp, E. A.; Vanmaekelbergh, D.; Meijerink, A. *J. Lumin*. **2000**, *87*, 454.
(34) Berry, F. J.; Laundy, B. J. *J. Chem. Soc., Dalton Trans*. **1981**, 1442.
(35) Nutz, T.; Haase, M. *J. Phys. Chem. B* **2000**, *104*, 8430.
(36) Falcony, C.; Garcia, M.; Ortiz, A.; Aloaso, J. C. *J. Appl. Phys*. **1992**, *72*, 1525.